Analysis of directional wave spectrum from simulated High Frequency Radar Sea echo

Duy-Toan Dao[1], Hwa Chien*[1], Kang-Hung Yang[2]

[1] Institute of Hydrological and Oceanic Sciences, National Central University, Taiwan (R.O.C.)

[2] Department of Industrial and Systems Engineering, Chung Yuan Christian University, Taiwan (R.O.C)

Abstract

The Central Weather Bureau (CWB) schedules to install three antenna array radar stations at northern islands of Taiwan for monitoring wave parameters, including directional ocean wave spectrum, significant wave height and period for the northern Taiwan Strait in 2019. Such systems use the beam-forming technique (BF) to acquire azimuthal information and can obtain more accurate 2nd order peaks in the Doppler-Range spectra, and thus makes it possible to provide the directional ocean wave spectral information. In present study, we implement the numerical simulations of the Doppler-Range spectra from bistatic HF Radar sea-echo based on the Barrick's equation (1972) and also the theory of Gill and Walsh (2001). The results are inter-compared with respect to the given directional wave spectrum and input parameters such as U10 and wind direction. The results show that the shape of the 2nd order Doppler-Range spectra can be influenced by the width of the 1st order peak. This simulation will be provided as a numerical tool to test and validate the inverse algorithms which estimate the wave spectrum from DR spectrum.

Key word: High Frequency ocean radar, Directional wave spectrum, Doppler spectral, Barrick's equation.

1. Introduction

The High frequency (HF) surface wave radar is currently the most common and widely applied land-based remote sensing technology of the ocean surface current, wave and wind mapping. Over the developments of four decades, this technique has been recognized as a robust tool in the monitoring of the coastal environment [9]. Two major receiving antenna types were adopted in the HF radar systems to determine the azimuthal directions of the backscattered signals, e.q. the cross-loop and antenna array. The former was used in the HF-CODAR system, which is selected by the Taiwan Ocean Research Institute (TORI) to be the main coastal radar systems around Taiwan island for surface current mapping. Nineteen HF CODAR systems along the coastline have been setup since 2009 and currently are in operational mode. The later features better accuracy of the data in-terms of S/N ratio compared to cross-loop type system, and thus can be used to give better resolved 2nd order information for wave field estimation. In order to fulfill the demands of surface wave monitoring for safety navigation purposes, the Central Weather Bureau (CWB) schedules to install three antenna array radar stations at the northern islands of Taiwan for monitoring wave parameters. It is highly needed to develop the methods for estimation of wave spectrum and parameters from antenna array signals. This study is the first step of the self-developing wave spectrum estimator from antenna array system. In present paper, we implement the forward numerical simulation of the Doppler-Range spectrum from given wave and wind fields. The fundamental theories were reviewed and introduced in this paper.

Two theories introduced in this paper are Barrick (1972) and Walsh & Gill (2001). Based on the investigation of the Bragg scattering mechanism by Crombie [1], Barrick [2] first successfully derived the equation described the relationship between the characteristic of monostatic radar cross section (RCS) and sea state parameter including current and directional wave spectrum. In 2000, Walsh and Gill [5] proposed a new analysis that was based upon a generalized function theory [15] and focused on the scattering electric field from the time-varying, good conducting ocean surface and involves a pulse dipole, and applied for the bistatic case. The comparison of two models was implemented by Walsh, and Gill [5]. Now, the bistatic model is not only applied to the new system of antenna array radar on the Ground but also to the system on a floating platform [14]. We repeat the comparisons in this study, too.

In order to retrieve the directional wave spectrum of the ocean surface, a number of methods have been developed based on the Barrick's equation for monostatic cases such as Wyatt [17], Howell and Walsh [11], Hashimoto [8]. In bistatic case, the first alternate analysis was implemented by Gill et. al. [6] based on the earlier work of Howell and Walsh [11]. In addition, Wyatt has published a method for processing data of antenna array [18]. It is the next step to implement those methods.

In this article, we first explained the different mechanism of Barrick's equation [2] and Walsh and Gill's approach [4]. Then, we describe step-by-step the simulation of the Doppler-range spectra of RCS of HF radar sea-echo data based on the approach of Gill and Walsh [4] with given directional wave spectrum, and presented in section 3. Finally, simulated results of two models will be compared and discussed in section 4.

2. Two Orders of Radar Cross Section

In the High frequency band, the sea surface can be seen as a slightly rough surface, the backscatter of HF radar signal from the sea surface can be analyzed based on the perturbation theory [4]. In the derivation, the ocean is first assumed to be in deep-water region and unbounded of the surface. Secondly, it provides high conductivity of sea water and less diffraction propagation attenuation of vertical polarization HF radio waves. In another word, the sea surface is considered as an ideal conductive surface, therefore the backscatter coefficients of vertical polarization can be deduced by the perturbation method. The vertical polarization part should be focused because the horizontally polarized component of scattering from the sea is several orders of magnitude lower than the vertical component [2].

The radar cross section (RCS) from the ocean surface, which based on the theory of E-M scattering from a rough surface, were developed using two methods i.e. the perturbation method and the Kirchhoff method. Typically, the RCS of HF radar sea-echo data is defined as the combination of the first-order (σ_1) and higher order (the second order, σ_2) spectra of Doppler-Range spectra. In which, the first-order cross section represents the interaction between radio waves and ocean waves having a wavelength one-half of the incidence E-M waves based on the theory of Resonance Bragg scattering [3], [4]. These peaks are related to ocean waves propagating outward or inward the radar site along the direction of radar looking. The second and higher-orders represent the double bounce effects, which is the interactions of radio wave with pairs or more of the ocean waves. It implies that the shape of ocean wave spectrum dominates the 2nd order Dopper-Range spectra. In addition, the nature of the scattered signal also depends on the radar operating frequency, beam width polarization and the type of configuration (monostatic or bistatic) [4].

Based on the boundary perturbation theory of Rice, Barrick firstly proposed the first-order of monostatic cross section for plane wave incidence casts the Bragg peaks as weighted delta functions [1]. After that, he extended that theory to the second-order in an attempt to investigate and explain the higher-order observed signals [2]. He also found out two contributions to this echo: the contribution of the hydrodynamic component due to the small nonlinear terms in the boundary conditions at the freeway water surface, and the contribution of the electromagnetic component due to the previously neglected high-order term of the boundary perturbational scatter theory [2]. The equations of two orders monostatic cross section are presented as:

$$\sigma_1(\omega_d) = 2^6\pi k_0^4 \sum_{m_2=\pm 1} S(-2m\boldsymbol{k}_0)\,\delta(\omega_d - m\omega_B) \quad (1)$$

$$\sigma_2(\omega_d) = 2^6\pi k_0^4 \sum_{m_1,\, m_2=\pm 1} \int_{-\infty}^{+\infty}\int_{-\infty}^{+\infty} S(m_1\boldsymbol{k}_1)S(m_2\boldsymbol{k}_2) \times |\Gamma|^2\delta\left(\omega_d - m_1\sqrt{gk_1} - m_2\sqrt{gk_2}\right)dpdq \quad (2)$$

In equation (1), $m_2 = \pm 1$ denotes the sign of the Doppler shift, $\boldsymbol{k}_0$ is the vector of radio waves, S(.) is the ocean wave spectrum, the Bragg frequency $\omega_B = \sqrt{2gk_0}$, $\delta(.)$ is the delta function constraint. In equation (2), $\boldsymbol{k}_1$ and $\boldsymbol{k}_2$ are two ocean wave vectors of magnitude k_1, k_2 and direction $\theta_{k_1}, \theta_{k_2}$ respectively on the coordinate p-q plane [13], Γ is the coupling coefficient that is the sum of the hydrodynamic term (Γ_H) and electromagnetic term (Γ_{EM}). According to the derivation of Barrick, two coupling coefficients are defined as [2]:

$$\Gamma_{EM} = \frac{1}{2}\left[\frac{(\boldsymbol{k}_1.\boldsymbol{k}_0)(\boldsymbol{k}_2.\boldsymbol{k}_0)/k_0^2 - 2\boldsymbol{k}_1.\boldsymbol{k}_2}{\sqrt{\boldsymbol{k}_1.\boldsymbol{k}_2} + k_0\Delta}\right] \quad (3)$$

$$\Gamma_H = \frac{-i}{2}\left[k_1 + k_2 + \frac{(k_1k_2 - \boldsymbol{k}_1.\boldsymbol{k}_2)(\omega_d^2 + \omega_B^2)}{m_1m_2\sqrt{\boldsymbol{k}_1.\boldsymbol{k}_2}(\omega_d^2 - \omega_B^2)}\right] \quad (4)$$

where, Δ is the normalized surface impedance value, and given by $\Delta = 0.011 - 0.012\text{i}$. The calculation and interpretation of monostatic cross section were implemented by Lipa and Barrick [13].

In 1980, Walsh [15] introduced a new analysis for radio scattering from rough surfaces based on the generalized function theory. His work focused on the scattered electric field from a random time-varying, high conductivity of the ocean surface and relates a pulse dipole source that leads to the use of the sampling function, instead of the Dirac delta function in the equation of radar cross sections. After that, Gill and Walsh [5] extended this analysis to include the bistatic case. Figure 1 described the bistatic scattering geometry for a single patch from the ocean surface, which is remote from Transmitter ($\mathbf{T_X}$) and Receiver ($\mathbf{R_X}$).

Based on the work of Walsh [15], Gill [4], Gill and Walsh [5], the scattered electric field from time-varying ocean surface is defined as [5]:

$$\mathrm{E}_n = (\mathrm{E}_n)_0 + (\mathrm{E}_n)_1 + (\mathrm{E}_n)_2 + \cdots \quad (5)$$

In equation (5), $(\mathrm{E}_n)_0$ is the zero-order term that represents the E-M wave propagation over a smooth plane surface. $(\mathrm{E}_n)_1$ is the first-order backscatter electric field, which is the sum of a single scatter of incident radiation from the first-order surface waves and a single scatter from a second-order surface component [5]. However, the second component of $(\mathrm{E}_n)_1$ will be appropriately addressed in the second-order terms from double scattering. $(\mathrm{E}_n)_2$ is the second-order backscatter electric field that is combined with three components: the second-order patch scatter filed components, $(\mathrm{E}_n)_{2P}$, the

second-order filed has a single scatter near the transmitter and another in patch scatter, $(E_n)_{2T}$, the second-order filed has a single scatter in patch scatter and another near the receiver $(E_n)_{2R}$. Whereas higher orders are neglected because their contribution is less important to the received E-field [5]. Therefore, the total received electric field is given as:

$$E_n \approx (E_n)_{11} + (E_n)_{2P} + (E_n)_{2T} + (E_n)_{2R} \quad (6)$$

In the next step, Gill (2001) determined the Doppler Power Spectral Density (PSD) of the received electric field based on a few statistical analyses as the ocean surface is statistical stationary and homogeneous during a single measurement, and its first-order Fourier coefficients are normally distribution. Given these assumptions, the autocorrelation of a random process will be a function only of the time shift. Therefore, it is convenient to express the autocorrelation of the field as the work in [5]. Finally, the HF bistatic cross sections from the ocean surface were derived from the Doppler PSD.

The first-order bistatic cross section, which associated with the first-order backscatter electric field of a single scatter of incident radiation, is presented as:

$$\sigma_{11}(\omega_d) = 2^4\pi k_0^2 \sum_{m=\pm 1} S(m\boldsymbol{k}) \frac{k^{\frac{5}{2}}\cos(\phi)}{\sqrt{g}} \times \Delta\rho_s Sa^2\left[\frac{\Delta\rho_s}{2}\left(\frac{k}{cos\phi} - 2k_0\right)\right] \quad (7)$$

where $\boldsymbol{k}$ is the wave vector of the ocean wave spectrum S(.), g is the gravity acceleration, k_0 is the wavenumber of radio signals, Sa(x) = sin[x]/x is the sampling function, $\Delta\rho_s$ is the patch width, ϕ is the bistatic angle. It is clear that $\sigma_{11}(\omega_d)$ is a maximum at $k = 2k_0 cos\phi$ and the Bragg peak are located at the Bragg frequency $\omega_B = \pm\sqrt{2gk_0 cos\phi}$ that has little different in compared with the same component in (1). Thus, equation (7) will reduce to similarly (1) if the patch width becomes infinite. However, for the finite of patch width, the first-order interaction becomes continuum that indicated the different of this model in compared with the earlier version [1].

The second-order cross section associated with the second-order backscatter electric field is presented [4], [5]. $\sigma_2(\omega_d) = \sigma_{2P}(\omega_d) + \sigma_{2P}(\omega_d) + \sigma_{2P}(\omega_d)$ (8) where, $\sigma_{2P}(\omega_d)$ is the second-order "patch scatter" cross section of two scatters occur on the remote elliptical scattering patch. $\sigma_{2T}(\omega_d)$ is the second-order cross section for the case of one scatter near $\mathbf{T_X}$ is followed by another on the remote patch, and $\sigma_{2R}(\omega_d)$ is the second-order cross section for the case of one scatter on the remote patch is followed by another near $\mathbf{R_x}$. It is clear that two last terms in (8) neglected in the Barrick's derivation. Fortunately, Gill and Walsh [5] pointed out that the second-order "patch scatter" cross section is main contributed to the total value of the second-order radar cross section, and it is presented as [5]:

$$\sigma_{2P}(\omega_d) = 2^3\pi k_0^2 \sum_{m_1=\pm 1}\sum_{m_2=\pm 1}\int_0^{\infty}\int_{-\pi}^{\pi}\int_0^{\infty} S(m_1\boldsymbol{k}_1) . S(m_2\boldsymbol{k}_2)\left|{}_S\Gamma_P\right|^2 k^2 cos\phi . \Delta\rho_s Sa^2\left[\frac{\Delta\rho_s}{2}\left(\frac{k}{cos\phi} - 2k_0\right)\right] . \delta\left(\omega_d + m_1\sqrt{gk_1} + m_2\sqrt{gk_2}\right) . k_1 dk_1 d\theta_{k_1} dk \quad (9)$$

where $\boldsymbol{k} = (2k_0 cos\phi, \theta_k)$ with the direction is the same with the direction of ellipse normal, $\theta_k = \theta_N$ as in Figure 1, and $\boldsymbol{k}$ is the sum of $\boldsymbol{k}_1$and $\boldsymbol{k}_2$ as in Figure 2a,b, the symmetrised coupling coefficient is defined by ${}_S\Gamma_P$, and given as ${}_S\Gamma_P = \left|{}_S\Gamma_E + \Gamma_H\right|$, ${}_S\Gamma_E$ and Γ_H are the symmetrised electromagnetic and the hydrodynamic coupling coefficients respectively, and are defined as [6], [4]:

$${}_S\Gamma_E = \frac{-j|\boldsymbol{k}_1 \times \boldsymbol{k}_2|^2}{2k^2\left[\sqrt{\boldsymbol{k}_1.\boldsymbol{k}_2} + (k_0\ \Delta)i\right]} \quad (10)$$

$$\Gamma_H = \frac{1}{2}\left\{k_1 + k_2 + \frac{g}{\sqrt{\omega_1\omega_2}}(k_1k_2 - \boldsymbol{k}_1.\boldsymbol{k}_2) \times \left[\frac{gk + (\omega_1+\omega_2)^2}{gk - (\omega_1+\omega_2)^2}\right]\right\} \quad (11)$$

where $\omega_1 = m_1\sqrt{gk_1}$ and $\omega_2 = m_2\sqrt{gk_2}$. Gill et. al., [6] suggested that there is only the hydrodynamic term which is dominant in the interest region of Doppler-Range spectral of RCS. Meanwhile, Huang et. al. [6] only considered the hydrodynamic coupling coefficient in the inverse problem. Equation (9) can reduce to similarly (2) when applying the Lathi's relationship [11] which will be presented in next section.

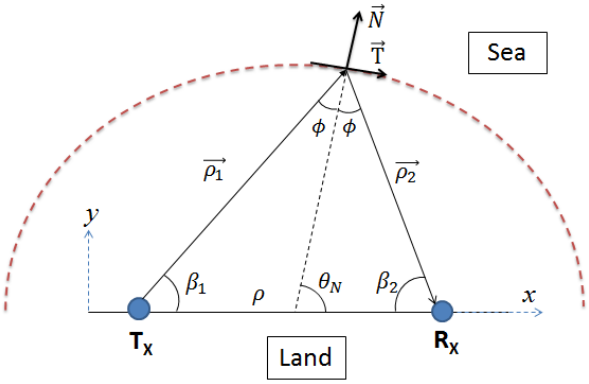

Figure 1. The general geometry of Bistatic Radar. $\vec{N}$ and $\vec{T}$ are the normal and tangent vector of the scattering ellipse. $\overrightarrow{\rho_1}$ and $\overrightarrow{\rho_2}$ are the vector of ρ_1 and ρ_2 that associate to the distant from T_x to scattering point and scattering point to R_X respectively

It is seen that there are several differences between the second-order equation of Barrick and those of Gill and Walsh's. Firstly, the existence of Sa(.) function associated with the pulse dipole source which may provides noise from system. Secondly, the direction of the normal vector of the scattering ellipse is changed an amount of ϕ in compared with the direction of incident waves from $\mathbf{T_X}$. Finally, the value of patch width and its effects to the width of major peaks from the Sa^2(.) function.

The second-order cross section component, $\sigma_{2T}(\omega_d)$, is presented as [5]:

$$\sigma_{2T}(\omega_d) = 2^2\pi k_0^2 \sum_{m_1=\pm1}\sum_{m_2=\pm1}\int_0^\infty\int_{-\pi}^{\pi}\int_0^\infty S(m_1\boldsymbol{k}_1) .S(m_2\boldsymbol{k}_2)\left|{}_E\Gamma_P\right|^2 k_2^2 cos\phi .\Delta\rho_s Sa^2\left[\frac{\Delta\rho_s}{2}\left(\frac{k_2}{cos\phi}-2k_0\right)\right] .\delta\left(\omega_d + m_1\sqrt{gk_1} + m_2\sqrt{gk_2}\right) .k_1 dk_1 d\theta_{k_1} dk_2 \quad (12)$$

where ${}_E\Gamma_P$ is the electromagnetic coupling coefficient that provides the main different between (9) and (12). As Gill mentioned [4], the main contribution of wave number k_2 in (12) is, due to the Sa(.) function, confined to the small value of $2k_0 cos\phi$. The value of $\sigma_{2T}(\omega_d)$ is much smaller than $\sigma_{2P}(\omega_d)$, and its reasons will be discussed in section 3.

The last second-order cross section component, $\sigma_{2R}(\omega_d)$, is presented as [5]:

$$\sigma_{2R}(\omega_d) = 2^2\pi k_0^2 \sum_{m_1=\pm1}\sum_{m_2=\pm1}\int_0^\infty\int_{-\pi}^{\pi}\int_0^\infty S(m_1\boldsymbol{k}_1) .S(m_2\boldsymbol{k}_2)\left|{}_E\Gamma_R\right|^2 k_1^2 cos\phi .\Delta\rho_s Sa^2\left[\frac{\Delta\rho_s}{2}\left(\frac{k_1}{cos\phi}-2k_0\right)\right] .\delta\left(\omega_d + m_1\sqrt{gk_1} + m_2\sqrt{gk_2}\right) .k_1 dk_2 d\theta_{k_2} dk_1 \quad (13)$$

where ${}_E\Gamma_R$ is the electromagnetic coupling coefficient that has replaced ${}_E\Gamma_T$ in (12). As the same above, the value of $\sigma_{2R}(\omega_d)$ is much smaller in compared with $\sigma_{2P}(\omega_d)$.

3. Calculation and interpretation of Bistatic Cross Sections

From the expression of Gill [4], the first-order cross section in equation (9) is replaced to here as:

$$\sigma_{11}(\omega_d) = 2^4\pi k_0^2 \sum_{m=\pm1} S(m\boldsymbol{k})\frac{k^{\frac{5}{2}}\cos(\phi)}{\sqrt{g}} \times \Delta\rho_s Sa^2\left[\frac{\Delta\rho_s}{2}\left(\frac{k}{cos\phi}-2k_0\right)\right] \quad (14)$$

Based on the derivation of Gill [4, chatter 3], it is clear that $\omega_d = -m_1\sqrt{gk}$.

Then $\begin{matrix}\omega_d < 0\,, & m_1 = 1\\ \omega_d > 0\,, & m_1 = -1\end{matrix}\Big\}$

From Figure 1, the value of bistatic angle will be changed in a different position of an elliptical patch, and the direction of ellipse normal also change belong to the area of patch scatter point. In this case, the direction of vector $\boldsymbol{k}$ (Fig. 2) along the outward ellipse normal, or $\theta_k = \theta_N$. When $\mathbf{T_X}$ and $\mathbf{R_X}$ are co-located, the value of the bistatic angle (ϕ) becomes to zero, then the bistatic case becomes the monostatic case. The size of scattering patch width ($\Delta\rho_s$) will be determined from given the pulse duration (τ_0) and the speed of light as $\Delta\rho_s = c\tau_0/2$. By the feature of the Sampling function, $Sa^2(.)$, in (9), the major peak of the first-order cross section is located at $\omega_d = \pm\sqrt{2gk_0 cos\phi}$. It indicated that the position of the first-order peak dependent on the operating frequency value and the bistatic angle that will be changed following the position on the scattering ellipse, which is observed by $\mathbf{T_X}$ and $\mathbf{R_X}$. In addition, the $Sa^2(.)$ factor presents a rapidly oscillating first order continuum and affects the shape of those peaks. However, the fluctuation of surface and noise effects make the signal varies as well as over time in the practical case. To provide a smoothing effect of this periodic behavior, there are some methods that could be applied such as Hamming window method [5], or Huang transform. The simulated result of the first order of bistatic radar cross sections will be discussed in section 4.

In order to calculate the Second-order bistatic cross section that was derived by Gill and Walsh [5], we first present the calculation of the $\sigma_{2P}(\omega_d)$ component that is the main contribution of the total second-order bistatic cross section [4], [5], [6]. This term represents the result of a single scatter from a second-order ocean wave and a double scatter from two first-order ocean waves which are near each other on the elliptical scattering patch. The calculation of the $\sigma_{2P}(\omega_d)$ is presented as (11):

$$\sigma_{2P}(\omega_d) = 2^3\pi k_0^2 \sum_{m_1=\pm1}\sum_{m_2=\pm1}\int_0^\infty\int_{-\pi}^{\pi}\int_0^\infty S(m_1\boldsymbol{k}_1) .S(m_2\boldsymbol{k}_2)\left|{}_S\Gamma_P\right|^2 k^2 cos\phi .\Delta\rho_s Sa^2\left[\frac{\Delta\rho_s}{2}\left(\frac{k}{cos\phi}-2k_0\right)\right] .\delta\left(\omega_d + m_1\sqrt{gk_1} + m_2\sqrt{gk_2}\right) .k_1 dk_1 d\theta_{k_1} dk \quad (15)$$

The relationship, which was proposed by Lathi [11],

$$\lim_{M\to\infty} MSa^2[Mx] = \pi\delta(x) \quad (16)$$

is applied to (15) when $\Delta\rho_s \to \infty$, then

$$\Delta\rho_s . Sa^2\left[\frac{\Delta\rho_s}{2}\left(\frac{k}{cos\phi}-2k_0\right)\right] = 2\pi cos\phi . \delta(k - 2k_0 cos\phi) \quad (17)$$

Insert (17) into (15), and invoke the first delta function to do the *dk* integral, give:

$$\sigma_{2P}(\omega_d) = 2^6\pi^2 k_0^4 cos^4\phi \sum_{m_1=\pm1}\sum_{m_2=\pm1}\int_0^\infty\int_{-\pi}^{\pi} S(m_1\boldsymbol{k}_1) .S(m_2\boldsymbol{k}_2)\left|{}_S\Gamma_P\right|^2 .\delta\left(\omega_d + m_1\sqrt{gk_1} + m_2\sqrt{gk_2}\right). k_1 dk_1 d\theta_{k_1} \quad (18)$$

It is clear that equation (18) is similar equation (2). The Doppler regions of the second-order are identical by the value of m_1 and m_2 in the delta function as:

$$\omega_d = -m_1\sqrt{gk_1} - m_2\sqrt{gk_2} \quad (19)$$

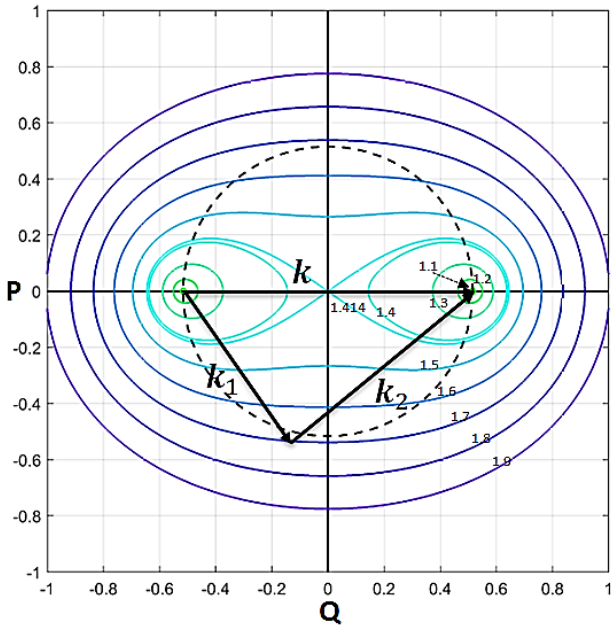

Figure 2a. Normalised frequency contours in case $m_1 = m_2$ *(the bistatic angle* $\phi = 10^0$*).*

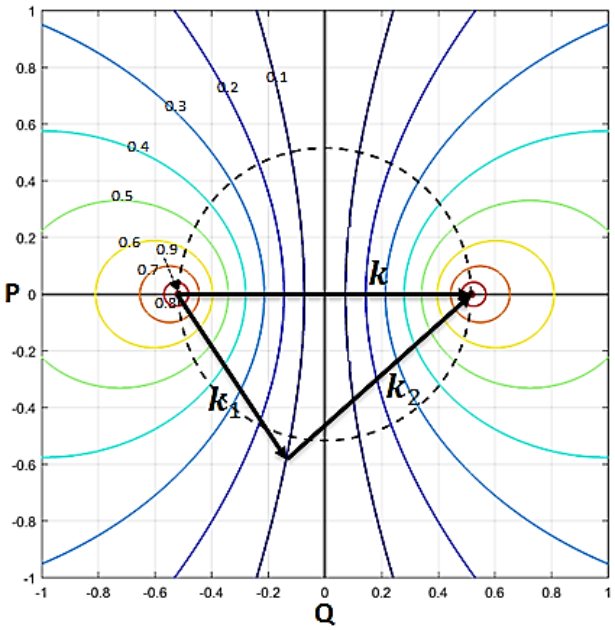

Figure 2b. Normalised frequency contours in case $m_1 \neq m_2$ *(the bistatic angle* $\phi = 10^0$*).*

<u>*Case 1:*</u> $m_1 = m_2$

Then, $\omega_d^2 = gk_1 + gk_2 + 2g\sqrt{k_1 k_2}$ (20)

From the triangle inequality in Fig 2, it showed that $k_1 + k_2 \geq k$ and $\sqrt{k_1 k_2} > 0$ referring to (20),

$\omega_d^2 > gk = 2gk_0 cos\phi = \omega_B^2$ (21)

gives $\omega_d < -\omega_B$, or $\omega_d > \omega_B$

It indicated that

$$\left.\begin{array}{l} \omega_d < -\omega_B\,,\ m_1 = m_2 = 1 \\ \omega_d > \omega_B\,,\ m_1 = m_2 = -1 \end{array}\right\} \quad (22)$$

The frequency contour of this case is plotted in Figure 2a. It showed that these contours are the same with those in monostatic case [13] even with the existence of bistatic angle. There are singularities in the radar spectrum at Doppler frequencies $|\omega_d| = \sqrt{2}\,\omega_B$ that is similar to the monostatic case. In Figure 2a, the dashed circle presents points which satisfy $\boldsymbol{k}_1.\boldsymbol{k}_2 = 0$, that is, the denominator in electromagnetic coupling coefficient is zero. It means the integral (18) has singularities will cause small peaks in the bistatic sea echo spectrum at the value of frequency [4],

$$|\omega_d| = \sqrt[4]{2^3 \frac{(1 \pm \sin\phi)}{cos^2\phi}}\,\omega_B \quad (23)$$

where, the frequency contours are tangential to the dashed circle.

<u>*Case 2:*</u> $m_1 \neq m_2$

Squaring (19) now gives the relationship

Then, $\omega_d^2 = gk_1 + gk_2 - 2g\sqrt{k_1 k_2}$ (24)

Proving in the same way as before, we have.

$\omega_d^2 < gk = 2gk_0 cos\phi = \omega_B^2$ (25)

It means $-\omega_B < \omega_d < \omega_B$

then, for $k_1 < k_2$

$$\left.\begin{array}{l} -\omega_B < \omega_d < 0\,,\ m_1 = -1, m_2 = +1 \\ 0 < \omega_d < \omega_B\,,\ m_1 = +1, m_2 = -1 \end{array}\right\} \quad (26a)$$

for $k_1 > k_2$

$$\left.\begin{array}{l} -\omega_B < \omega_d < 0\,,\ m_1 = +1, m_2 = -1 \\ 0 < \omega_d < \omega_B\,,\ m_1 = -1, m_2 = +1 \end{array}\right\} \quad (26b)$$

The frequency contours of this case are plotted in Figure 2b. It shows that frequency contours are not tangential to the dashed circle, so the integrable singularity resulting from the electromagnetic term does not exist, and secondary peaks do not appear in the region between the Bragg lines of the second-order bistatic cross section.

To simulate the RCS of HF radar sea-echo, the double integration of the second-order of Doppler-Range spectra should be simplified as [4], [13]. In Figure 2a,b, the frequency contour is symmetrized via the P and Q axis of the P-Q plane. Therefore, we took the integral only the left plan ($k_1 < k_2$) and double the results (Figure 2a,b). The value of second-order radar cross section will be computed with given value of the first ocean vector ($\boldsymbol{k}_1$), which satisfies the condition of delta function constraints in (15) and (18), and its direction (θ_{k_1}).

From Figure 2a, the relationship between k_1 and k_2 is identical based on the law of cosines and sines in triangle as [4],

$$k_2 = \sqrt{k_1^2 - 2k_1 k cos\theta_1 + k^2} \quad (27)$$

$$\theta_{k_2} = 2\pi - sin^{-1}\left(\frac{k_2 sin\theta_1}{k_1}\right) \quad (28)$$

where $\theta_{\boldsymbol{k}_1}$, $\theta_{\boldsymbol{k}_2}$ are the direction of vector $\boldsymbol{k}_1$ and $\boldsymbol{k}_2$ in the coordinate P-Q respectively. From figure 1, 2, the direction of axis P must be the same with the direction of elliptical normal of scattering patch, or $\theta_k = \theta_N$ in the coordinate Oxy.

Thus, it is easy to simplify one of the integrations using the delta function constraint on the variables that were presented by Lipa and Barrick [13] for monostatic cross sections. The definition of new variables as follows:

$$y = \sqrt{k_1} \tag{29}$$

then, $k_1 dk_1 = 2y^2 dy$ (30)

and the delta function constrain is presented in form

$$\delta(.) = \delta\left(\omega_d + D_P(y, \theta_{\boldsymbol{k}_1})\right) \tag{31}$$

where, using (28), gives

$$y = \frac{m_1 D_P\left(y, \theta_{\boldsymbol{k}_1}\right) - L\left[\sqrt{g}(y^4 - 2y^2 k cos\theta_1 + k^2)^{1/4}\right]}{\sqrt{g}} \tag{32}$$

Then, for a given $\theta_{\boldsymbol{k}_1}$

$$dy = \left|\frac{\partial y}{\partial D_P}\right|_{\theta_{\boldsymbol{k}_1}} dD_P \tag{33}$$

with the Jacobian of the transformation, using L = $m_1 m_2$, give as

$$\left|\frac{\partial y}{\partial D_P}\right|_{\theta_{\boldsymbol{k}_1}} = \frac{1}{\sqrt{g}\left[1 + \frac{L(y^3 - yk cos\theta_1)}{(y^4 - 2y^2 k cos\theta_1 + k^2)^{3/4}}\right]} \tag{34}$$

Applying the transformation, (18) is written as

$$\sigma_{2P}(\omega_d) = 2^7 \pi^2 k_0^4 cos^4\phi \sum_{m_1=\pm1} \sum_{m_2=\pm1} \int_{-\pi}^{\pi} \int_{D_P} S(m_1 \boldsymbol{k}_1) . S(m_2 \boldsymbol{k}_2) \left|{}_S\Gamma_P\right|^2 \delta\left(\omega_d + D_P(y, \theta_{\boldsymbol{k}_1})\right) . y^3 \left|\frac{\partial y}{\partial D_P}\right|_{\theta_{\boldsymbol{k}_1}} dD_P d\theta_{k_1} \tag{35}$$

It is clear that the limits on the D_P integral could be defined from (31) which depends on the value of m_1 and m_2 under consideration that was illustrated in (22) and (24). In general, the delta function constraint is solved using numerical methods. It means

$$G(y) = \omega_d + D_P\left(y, \theta_{\boldsymbol{k}_1}\right) \tag{36}$$

, and there exists a solution $y = y^*$ such that $G(y^*) = 0$. Thus, (36) can be solved numerically using the Newton-Raphson method [4], [13]. In which, a suitable initial guess for the whole integral is defined as:

$$y^* = \frac{-m_1(\omega_d + m_2\omega_B)}{\sqrt{g}} \tag{37}$$

The calculation of the symmetrised coupling coefficient is presented in (10) and (11). Finally, all of the features of the integral in (35) that are used to calculate the second-order "patch" cross section have presented.

Secondly, we mentioned about the features of the $\sigma_{2T}(\omega_d)$ term of the second-order bistatic cross section. As we explained before, this term represents the Doppler cross section component involving one scatter near $\mathbf{T_x}$ followed by another on the remote patch [4], [5]. Applying the same technique for the $Sa^2(.)$ function in (12), we have,

$$\sigma_{2T}(\omega_d) = 2^5 \pi^2 k_0^4 cos^4\phi \sum_{m_1=\pm1} \sum_{m_2=\pm1} \int_{-\pi}^{\pi} \int_{0}^{\infty} S(m_1 \boldsymbol{k}_1) . S(m_2 \boldsymbol{k}_2) \left|{}_E\Gamma_T\right|^2 . \delta\left(\omega_d + m_1\sqrt{gk_1} + m_2\sqrt{gk_2}\right) . k_1 dk_1 d\theta_{k_1} \tag{38}$$

where, $\boldsymbol{k}_2 \approx \boldsymbol{k}$, it means the $S(m_2\boldsymbol{k}_2)$ is the spectrum of only two waves having wave length $2k_0 cos\phi$ and travelling inner and outer along the ellipse normal, ${}_E\Gamma_T$ is the electromagnetic coupling coefficient. For HF operating frequencies, ocean waves have wavelength $2k_0 cos\phi$ located at the end of the energy spectrum that makes the $\sigma_{2T}(\omega_d)$ which becomes less important as compared to the $\sigma_{2P}(\omega_d)$ [4].

To calculate the value of the $\sigma_{2T}(\omega_d)$, we first define the Doppler Regions under the consideration of m_1 and m_2. To satisfy the delta function in (38), it is required as:

$$\omega_d = -m_1\sqrt{gk_1} - m_2\sqrt{gk_2} = -m_1\sqrt{gk_1} - m_2\sqrt{2gk_0 cos\phi} \tag{39}$$

insert $\omega_B = \sqrt{2gk_0 cos\phi}$, and applying the same way as previous, we have [4],

$$\left.\begin{array}{ll} \omega_d < -\omega_B\,, & m_1 = +1, m_2 = +1 \\ -\omega_B < \omega_d < 0, & m_1 = -1, m_2 = +1 \\ 0 < \omega_d < \omega_B\,, & m_1 = +1, m_2 = -1 \\ \omega_d > \omega_B\,, & m_1 = -1, m_2 = -1 \end{array}\right\} \tag{40}$$

The new variable is defined as $y = \sqrt{k_1}$, as previous, insert (30), gives

$$\delta(.) = \delta(\omega_d + D_T(y)) \tag{41}$$

Where

$$y = \frac{m_1 D_T(y) - L\omega_B}{\sqrt{g}} \tag{42}$$

the Jacobian of the transformation is

$$\left|\frac{\partial y}{\partial D_T}\right| = \frac{1}{\sqrt{g}} \tag{43}$$

Applying the transformation, (38) is written as

$$\sigma_{2T}(\omega_d) = 2^5 \pi^2 k_0^4 cos^4\phi \sum_{m_1=\pm1} \sum_{m_2=\pm1} \int_{-\pi}^{\pi} \int_{0}^{\infty} S(m_1 \boldsymbol{k}_1) . S\left(2k_0 cos\phi, \theta_N + \left(\tfrac{1-m_2}{2}\right)\pi\right) . \left|{}_E\Gamma_T\right|^2 \delta(\omega_d + D_T(y)) . \frac{y^3}{\sqrt{g}} dD_P d\theta_{k_1} \tag{44}$$

The solution, y^*, is directly calculated from delta function as

$$y^* = \frac{-(\omega_d + m_2\omega_B)}{m_1\sqrt{g}} \tag{45}$$

The electromagnetic coupling coefficient in (38) is presented as follows [5]:

$${}_E\Gamma_T = \left\{\frac{\boldsymbol{k}_1.(\boldsymbol{k}_1 + k_0\widehat{\boldsymbol{\rho}}_1)}{\sqrt{\boldsymbol{k}_1.(\boldsymbol{k}_1 + 2k_0\widehat{\boldsymbol{\rho}}_1)}}\right\} . \left\{\frac{-k_0^2 - jk_0\sqrt{\boldsymbol{k}_1.(\boldsymbol{k}_1 + 2k_0\widehat{\boldsymbol{\rho}}_1)}}{k_0^2 + \boldsymbol{k}_1.(\boldsymbol{k}_1 + 2k_0\widehat{\boldsymbol{\rho}}_1)}\right\} \tag{46}$$

where, $\widehat{\boldsymbol{\rho}}_1$ is the unit vector associated with vector $\boldsymbol{\rho}_1$ in Figure 1. Gill [5] suggested that singularities occur in

${}_E\Gamma_T$ when $\boldsymbol{k}_1.(\boldsymbol{k}_1 + 2k_0\widehat{\boldsymbol{\rho}}_1) = 0$, and he found that the singularities will appear at the Doppler frequencies that are given from (39) [5].

$$\omega_d = -m_1\sqrt{2gk_0} - m_2\omega_B = \omega_B\left\{-m_2 - \frac{m_1}{cos\phi}\right\} \quad (47)$$

when $m_1 = m_2 = \pm 1$, these Doppler frequencies are $\mp\omega_B\{1 + 1/\sqrt{cos\phi}\}$ respectively. In contrast, $m_1 \neq m_2$ there are two peaks removed close to zero Doppler frequency by an amount which depends on the value of bistatic angle. Then, the $\sigma_{2T}(\omega_d)$ can be calculated from all of these features of integral (44) which have presented above.

Finally, we expressed the features of the last component, which is the $\sigma_{2R}(\omega_d)$, of the second-order bistatic cross section. Thus, this component represents the Doppler cross section component involving one scatter in remote patch followed by another one near $\mathbf{R_x}$ [4], [5]. We applied the same technique for the $Sa^2(.)$ function in (13), we have,

$$\sigma_{2R}(\omega_d) = 2^5\pi^2k_0^4cos^4\phi \sum_{m_1=\pm1}\sum_{m_2=\pm1}\int_{-\pi}^{\pi}\int_0^{\infty} S(m_1\boldsymbol{k}_1) .S(m_2\boldsymbol{k}_2)\left|{}_E\Gamma_R\right|^2 .\delta\left(\omega_d + m_1\sqrt{gk_1} + m_2\sqrt{gk_2}\right) .k_2dk_2d\theta_{\boldsymbol{k}_2} \quad (48)$$

where, $\boldsymbol{k}_1$ associated with the scatter on the remote patch, is fixed in magnitude and direction as $k_1 \approx 2k_0cos\phi$ and $\theta_{\boldsymbol{k}_1} = \theta_{\vec{N}}$ respectively. In contrast, $\boldsymbol{k}_2$ that is linked to a wave of ocean surface near the receiver can assume any direction from –π to π. The magnitude of $\boldsymbol{k}_2$ can be determined based on the satisfaction of the delta function. ${}_E\Gamma_R$ is the electromagnetic coupling coefficient near the receiver. As the same with $\sigma_{2T}(\omega_d)$, the $\sigma_{2R}(\omega_d)$ also becomes secondary importance as compared to the $\sigma_{2P}(\omega_d)$ [4].
From the delta function of (45), it is required as

$$\omega_d = -m_1\sqrt{gk_1} - m_2\sqrt{gk_2} = -m_1\sqrt{2gk_0cos\phi} - m_2\sqrt{gk_2} \quad (49)$$

Using $\omega_B = \sqrt{2gk_0cos\phi}$, and applying the same expression as before, we have [4],

$$\left.\begin{array}{l} \omega_d < -\omega_B\,, \quad m_1 = +1, m_2 = +1 \\ -\omega_B < \omega_d < 0,\ m_1 = +1, m_2 = -1 \\ 0 < \omega_d < \omega_B\,,\ m_1 = -1, m_2 = +1 \\ \omega_d > \omega_B\,, \quad m_1 = -1, m_2 = -1 \end{array}\right\} \quad (50)$$

Letting a new variable $y = \sqrt{k_2}$, and insert (30), gives

$$\delta(.) = \delta(\omega_d + D_R(y)) \quad (51)$$

Where

$$y = \frac{m_2D_R(y) - L\omega_B}{\sqrt{g}} \quad (52)$$

The Jacobian of the transformation is presented as

$$\left|\frac{\partial y}{\partial D_R}\right| = \frac{1}{\sqrt{g}} \quad (53)$$

Then, (41) is written as:

$$\sigma_{2R}(\omega_d) = 2^5\pi^2k_0^4cos^4\phi \sum_{m_1=\pm1}\sum_{m_2=\pm1}\int_{-\pi}^{\pi}\int_0^{\infty} S(m_2\boldsymbol{k}_2) .S\left(2k_0cos\phi, \theta_N + \left(\frac{1-m_1}{2}\right)\pi\right) .\left|{}_E\Gamma_R\right|^2\delta(\omega_d + D_R(y)) .\frac{y^3}{\sqrt{g}}dD_Rd\theta_{\boldsymbol{k}_2} \quad (54)$$

The solution, y^*, is simply calculated from delta function as

$$y^* = \frac{-(\omega_d + m_1\omega_B)}{m_2\sqrt{g}} \quad (55)$$

The value of ${}_E\Gamma_R$ in (48) is computed as [5]:

$${}_E\Gamma_R = \left\{\frac{k_0\boldsymbol{k}_2.\widehat{\boldsymbol{\rho}}_2}{\sqrt{\boldsymbol{k}_2.(\boldsymbol{k}_2 - 2k_0\widehat{\boldsymbol{\rho}}_2)}}\right\} \quad (56)$$

where, $\widehat{\boldsymbol{\rho}}_2$ is the unit vector associated with vector $\boldsymbol{\rho}_2$ in Figure 1. According to the work of Gill [4], the circle of singularities correspond to the satisfaction of $\boldsymbol{k}_2.(\boldsymbol{k}_2 - 2k_0\widehat{\boldsymbol{\rho}}_2) = 0$, and he pointed out that these singularities occur at Doppler frequencies which are given from (49) [5].

$$\omega_d = -m_1\omega_B - m_2\sqrt{2gk_0} = \omega_B\left\{-m_1 - \frac{m_2}{cos\phi}\right\} \quad (57)$$

when $m_1 = m_2 = \pm 1$, these spectral peaks may be located at $\mp\omega_B\{1 + 1/\sqrt{cos\phi}\}$ respectively. For $m_1 \neq m_2$, there are two more peaks removed near zero Doppler frequency by an amount that depends on $cos\phi$. It is clear that both $\sigma_{2T}(\omega_d)$ and $\sigma_{2R}(\omega_d)$ have theoretical peaks in the same location of Doppler frequency. Finally, the $\sigma_{2R}(\omega_d)$ is calculated from the integral in (54).

This section, we have presented the calculation of the bistatic cross section that was developed by Gill and Walsh [5]. In next section, we will discuss the dependence of Doppler spectra on such factors as the bistatic geometry parameters, wind condition and the operating radar frequency.

4. Simulated results and Comparison

To prove the argument in section 3, we first do the sensitivity test to evaluate the effect of input parameters to simulated results of RSC. The JONSWAP spectrum and a cardioids directional factor are chosen to represent the ocean spectrum and spreading respectively.

$$S(\boldsymbol{k}) = S(k)G(\theta_k) \quad (58)$$

The JONSWAP spectrum is presented as:

$$S(k) = \frac{g^2}{2^5\pi^4gf^3}S(f) \quad (59)$$

Where S(f) is the one-dimension frequency spectra, is given [9],

$$S(f) = \frac{\alpha g^2}{(2\pi)^4f^5}\exp\left(-\frac{5}{4}\left(\frac{f}{f_m}\right)^4\right)\gamma^{exp\left(\frac{-(f-f_m)^2}{2\sigma^2f_m^2}\right)} \quad (60)$$

In equation (60), f_m is the peak frequency, α is the energy scale, γ is the shape parameter, σ develops as the spectrum develop which depends on the aspect of fetch-limited spectra. The last part of (60) is the function of fetch and duration. In this study, we assumed the

parameter of JONSWAP spectrum that was taken in a fully developed limited as in [15].

The cardioids directional distribution is chosen as Lipa and Barrick [13], and is presented,

$$G(\theta_k) = \frac{4}{3\pi} cos^4\left(\frac{\theta_k - \theta_w}{2}\right) \quad (61)$$

where θ_k is the direction of vector $\boldsymbol{k}$ of sea waves, and θ_w is the direction of wind.

According to the setup of the antenna array radar station in NCU coastal station at Yong-An, northwestern coast of Taiwan. It is assumed that distant between $\mathbf{T_X}$ & $\mathbf{R_X}$ is 2 km. As both T_X and R_X will be installed along the coastline, the direction from the transmitter to the receiver is approximately 30^0 to the North. the distance from the scattering point to T_X and R_X are the same ($\rho_1 = \rho_2 = 10$km). Let the radar operating frequency to be 25 MHz, and the pulse duration of 150 kHz, the patch width $\Delta\rho_s$= 1000 m. The simulation results are shown as follows.

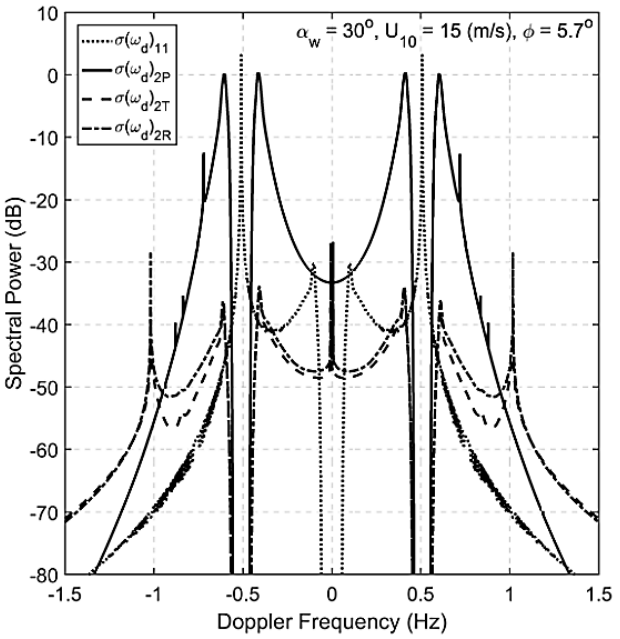

Figure 3. An example of the components of the bistatic cross section.

Figure 3 shows an example of the component of the bistatic cross section with given JONSWAP spectrum, U_{10} 15 m/s, wind direction θ_w of 30^0. The value of the bistatic angle, ϕ, is approximately 6^0. It is clear that the first-order cross section $\sigma(\omega_d)_{11}$ in Gill and Walsh's model is the continuum, and have contributed to the total value of RCS. It leads to some problems: the estimated directional spectrum from the second-order of RCS will be different to the target directional spectrum, and the width of the first-order peak, which due to the feature of the $Sa^2(.)$ function and the amount of patch width, may make it close and attached to the second-order component. Therefore, it could be difficult to determine the position and exact value of the second-order radar cross section. Fortunately, we can quantitatively evaluate the contribution of the $\sigma(\omega_d)_{11}$ into the total RCS through simulated results. From Figure 3, we can see that there exists the integral singularities that contained in three second-order components at Doppler frequency as mentioned in (23), (47) and (57). In addition, it is easily seen that both $\sigma_{2T}(\omega_d)$ and $\sigma_{2R}(\omega_d)$ are much smaller than the value of $\sigma_{2P}(\omega_d)$. Therefore, two last components in (8) may be neglected in the inverse work.

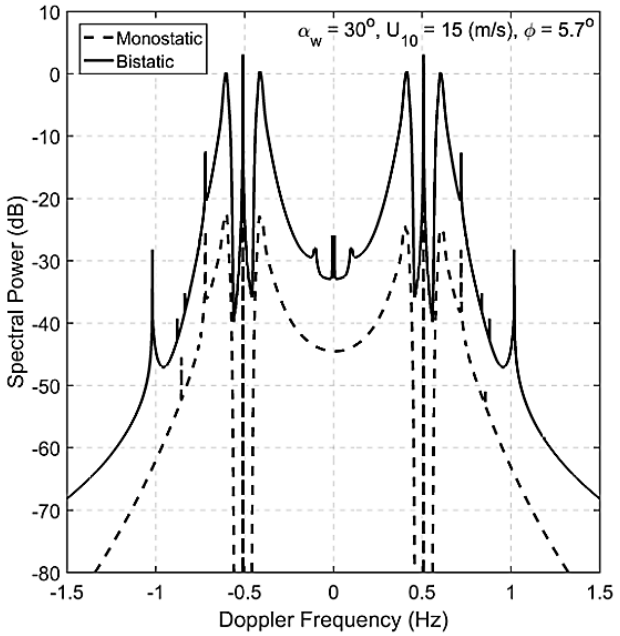

Figure 4. An example of the comparison between the bistatic cross section and the monostatic cross section which were proposed by Gill and Walsh and Barrick respectively.

In Figure 4, the difference between the RCS of Barrick's model and Gill & Walsh's model is presented. In Barrick's model, the first-order term was separated from the second-order term based on the delta function constraints. In Figure 4, we see that there is quite comparable between the left and the right parts of the bistatic cross section, but in monostatic case, the second-order cross session of left part is higher than the right part. It causes by the different direction of two scattering ellipse normal vectors which equal the value of bistatic angle. The integral singularities contained in the second-order of RCS located at different Doppler frequency following (23), (47), (57) and [12, page 16], except at Doppler frequency $\omega_d = \sqrt{2}\omega_B$. In addition, the value of RCS of Barrick's model is lower than those of Gill & Walsh model, because of the presence of $Sa^2(.)$ function and patch width in (7), (9), (12) and (13).

Figure 5 shows the effect of different input of wind direction to the value of RCS in the bistatic case. The equivalence between the RSC of the positive part or negative of Doppler frequency depends on the angle between wind direction and the direction of scattering ellipse normal vector. Because of the symmetry, the RCS

in negative part will be bigger than those of positive part if the angle is in a range of [-90^0 ~ 90^0]. In contrast, the RCS in positive part will be bigger than those of negative part when the absolute value of this angle larger than 90^0. For the example in figure 5, the direction of the normal vector of scattering ellipse is 300^0 in compared with the north direction.

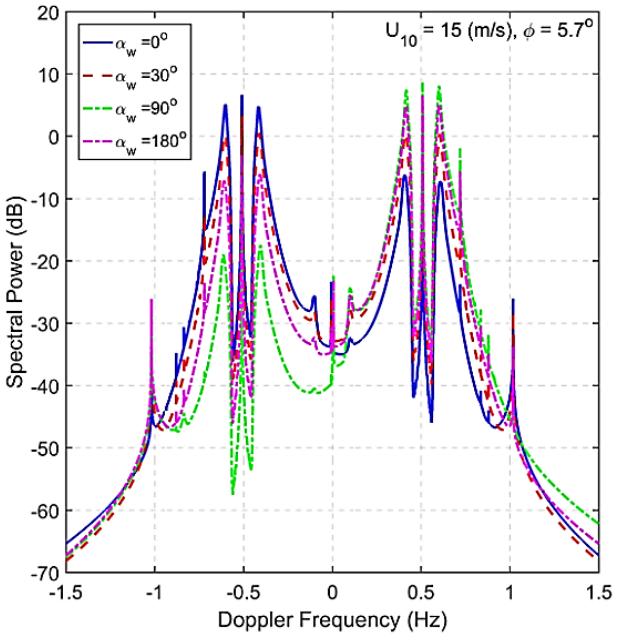

Figure 5. An example of the comparison of the bistatic cross section with the different input value of wind direction.

The effect of different given wind speeds to the value of RCS in the bistatic case is shown in Figure 6. It is clear that the value of RCS increases in general and significant around the second-order peaks that correspond to the increase of wind speed. Because wind speed is a very important parameter in spectrum model that contribute to the value of the second-order of RCS. This trend is similar those of the monostatic case.

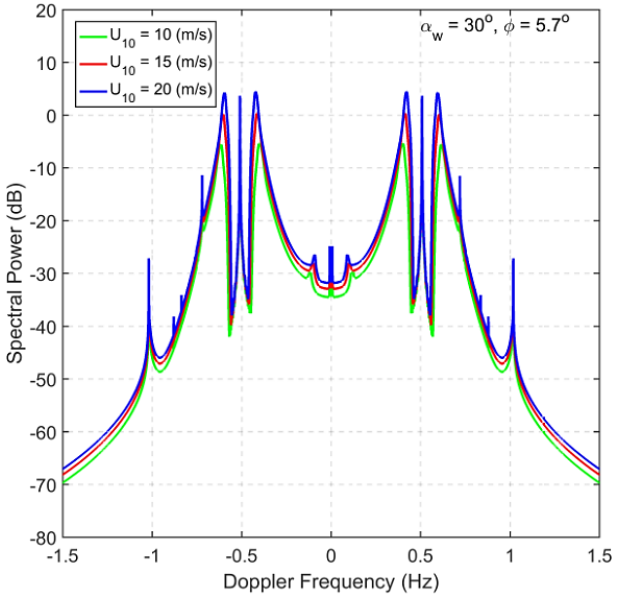

Figure 6. An example of the comparison of the bistatic cross section with the different input value of wind speed.

5. Conclusion

Based on the work of Barrick [1], [2], Gill and Walsh [5], the radar cross section of two model are conducted and compared. The first-order of the bistatic cross section is the continuum, and depends on the finite width of the signal pulse, which shows the difference in compared with the earlier model. The second-order of the bistatic cross section in Gill and Walsh's approach was added possible scattering terms near transmitter and receiver antennas, which neglected in the earlier monostatic version. In addition, the first-order terms could be added into the regions of the second-order term in practical. That can lead to the estimated directional spectrum from the second-order cross section may be different with given directional spectrum of input step. However, we can quantitatively the contribution of the first-order components through the sensitivity test of simulation work.

The effect of different input parameters of wind speed and wind direction is evaluated through simulation results. The change of RSC in the bistatic case is similar with those of the monostatic case.

In this study, we have done the simulation work of the radar cross section of HFR sea-echo. Besides that, the simulation work will be helpful for the inverse problem. In future work, the inversion algorithm will be implemented to retrieve the directional wave spectrum from the simulated Doppler spectral.

6. Reference

[1] Barrick, D.E., "First-order theory and analysis of MF/HF/VHF scatter from the sea," IEEE Transaction on Antenna and Propagation, Vol. 20, pp. 2-10, 1972.

[2] Barrick, D.E. (1972a) "Remote sensing of sea state by radar," *Remote Sensing of the Troposphere*, edited by V. Derr, chap. 12, pp. 1-46, U.S. Govt. Print. Off., Washington. 1972.

[3] Crombie, D., "Doppler spectrum of sea echo at 13.56 mc./s," *Nature*, Vol. 175, No. 459, pp. 681-682, 1959

[4] Gill, E.W. "The Scattering of High Frequency Electromagnetic Radiation from the Ocean Surface: An Analysis Based on a Bistatic Ground Wave Radar Configuration", *PhD thesis*, Memorial University of Newfoundland, 1999.

[5] Gill, E.W. and Walsh, J. "High-frequency bistatic cross section of the ocean surface," *Radio Science*, Vol. 36, No. 6, pp. 1459-1475, 2001.

[6] Gill, E.W. et. al., , "An Alternative Analysis for the Second-order High Frequency Bistatic Radat Cross Section of the Ocean Surface-Patch Scatter and its Inversion," *Oceans 2003 MTS/IEEE*, San Diego, USA, pp. 20336-2340, 2003.

[7] Gill, E.W., Huang, W., Walsh, J., "The Effect of the Bistatic Scattering Angle on the High Frequency Radar Cross Sections of the Ocean Surface," *IEEE Geoscience and Remote Sensing letters*, Vol. 5, No. 2, pp 143-146, 2008.

[8] Hashimoto, N., K. Kobune and Y. Kameyama., "Estimation of directional spectrum using the Bayesian approach and its application to field data analysis," Report of P.H.R.I, Vol. 26, No. 5, pp.57-100, 1987.

[9] Hasselman, K. et al., "Measurement of wind-wave ground and swell decay during the Joint North Sea Wave Project (JONSWAP)," Dtsch. Hydrogh. Z., Suppl. A, 8, 12, 95pp. 1973.

[10] Heron, M., et. al., "Application of HF Radar I Hazard Management", edited by Huang, W., *International Journal of Antennas and Propagation*, Vol. 2016

[11] Howell.R. and Walsh. J., "Measurement of Ocean Wave Spectra Using Narrow-Beam HF radar," *IEEE Journal of Oceanic Engineering*, Vol. 18, No. 3, pp. 296-305, 1993.

[12] Lathi, B., "Random Signal and Communication Theory," Scranton, Penn.: International Textbook Company, 1968.

[13] Lipa, B.J. and Barrick. D.E., "Analysis methods for narrow-beam High frequency radar sea echo," *NOAA Techniqual Report EDL* 420-WPL 56, 1982.

[14] Walsh, J., Huang, W., Gill, E.W., "The Second-Order High Frequency Radar Ocean Surface Cross Section for Antenna on a Floating Platform," *IEEE Transaction on Antenna and Propagation*, Vol. 60, No. 10, pp 4804-4813, 2012.

[15] Walsh, J., Donelly, R., "A new technique for studying propagation and scattering for mixed paths with discontinuities," Proc. Royal Society of London, Vol. A 412, pp. 152-167. 1987

[16] Walsh, J., "On the theory of electromagnetic propagation across a rough surface and calculation in the VHF region," OEIC Report N00232, Memorial University of Newfoundland, St. John's, Newfoundland, 1980.

[17] Wyatt, L. R., "A relaxation method for integral inversion applied to HF radar measurement of the ocean wave directional spectrum," Int. J. Remote Sensing, Vol. 11, No. 8, pp. 1481-1494, 1990.

[18] Wyatt, L. R., "Limits to inversion of HF radar backscatter for ocean wave measurement," Journal of Atmospheric and Oceanic Technology, Vol. 17, No.12, pp. 1651-1665, 1990.